Optica Applicata, Vol. XLIX, No. 2, 2019
DOI: 10.5277/oa190213

Two-step dual-wavelength interferometry for surface relief retrieval

ARKADY B. KMET' LEONID I. MURAVSKY*, TARAS I. VORONYAK, IHOR V. STASYSHYN

Karpenko Physico-Mechanical Institute of the NAS of Ukraine,
5 Naukova St., 79060 Lviv, Ukraine

*Corresponding author: muravskyleon@gmail.com, murav@ipm.lviv.ua

The new two-step dual-wavelength interferometry method that uses only two pairs of interferograms for surface relief retrieval is proposed. In this method, two interferograms in each pair are differed only by an arbitrary phase shift of a reference wave. The method allows using only one out-of-plane shift of a reference wave to record each second interferogram in both pairs, since arbitrary phase shifts between interferograms in each pair can be defined by calculation of the correlation coefficient between two interferograms. This method can extract separately areal surface roughness and areal waviness phase maps from a phase map of the total surface relief and reduce errors produced during the surface relief retrieving. Computer simulation and experimental verification have confirmed the reliability of the proposed method.

Keywords: dual-wavelength interferometry, two-step phase shifting interferometry, blind phase shift, surface relief retrieval, areal surface roughness, areal waviness, phase map.

1. Introduction

Dual-wavelength (DW) phase shifting interferometry (PSI) is successfully used for enlargement of a measurement rate of surface relief heights [1, 2]. In single-wavelength PSI techniques, the 2π ambiguity problem does not allow us to reconstruct the surface relief if the phase jump $\Delta\varphi_p$ between adjacent pixels is larger than π. If a two-beam interferometer with the normal incidence of light on an object plane is used, such jump corresponds to height jump Δh_p larger than $\lambda/4$ because $\Delta h_p = \lambda(\Delta\varphi_p)/4\pi$.

DW PSI allows expanding a range of surface height measurement due to using a synthetic wavelength

$$\Lambda = \frac{\lambda_1 \lambda_2}{|\lambda_1 - \lambda_2|} \tag{1}$$

and the retrieved height jumps can be increased theoretically in Λ/λ_1 or Λ/λ_2 times [1].

Though DW PSI techniques have been already developed throughout three decades, the problem of elimination of the noise which is increased about Λ/λ_1 or Λ/λ_2 times in the synthesized phase map (PM) remains actual. There are some approaches to suppress these noises. PARSHALL and KIM [3] have proposed to produce a coarse PM which is free of discontinuities and possesses a longer range (in Λ/λ_1 or Λ/λ_2 times), to suppress an amplified noise, and finally to synthesize the fine map. TAY *et al*. [4] have proposed the similar ideology with using an algorithm of phase error correction combined with windowed Fourier filtering. XU *et al*. [5] have developed a new method of DW in-line PSI, which allows to acquire two dc-term-suppressed intensities with a 2π phase shift. However, phase shifting errors inherent in this method led XU *et al*. to develop a new DW iterative method with arbitrary phase shifts [6]. Another problem is caused by the necessity to produce in DW PSI twice as many interferograms as in single wavelength PSI. For example, KUMAR *et al*. [7] have used a seven-phase step algorithm for both wavelengths to reconstruct 3D surface profiles with the help of a DW sequential illumination technique.

We propose a new two-step dual-wavelength interferometry method (TS DWIM), which uses only two pairs of interferograms for surface relief (texture) retrieval. Each pair is produced for one of two wavelengths λ_1 or λ_2, and two interferograms in each pair are differed only by an arbitrary phase shift of a reference wave. Because the method does not need phase shift calibration, it is enough to use only one phase shift to record both pairs of interferograms. Therefore, this method can ensure fast registration of all four interferograms, suppressing simultaneously the noise in a synthesized PM.

The necessity to develop the TS DWIM was initiated as a result of numerical experiments with polished smooth surfaces of CT-notched specimens near the notch root [8, 9] during fatigue. Different types of materials were studied for determination of both a fatigue process zone (FPZ) dimensions including its size d^*, and dimensions of monotonic and cyclic plastic zones with the help of a two-step interferometry method with blind phase shift of a reference wave (method 1) [10] and a method for evaluation of the FPZ dimension (method 2) that is based on a two-stage procedure of a surface relief retrieval including areal (3D) surface roughness and waviness extraction [9]. Methods 1 and 2 allow retrieving the 3D surface relief with RMS value $S_q \le \lambda/10$ and provide definition of the above mentioned mechanical characteristics for cyclically soften materials. These characteristics were also determined by the method 2 for some materials possessing moderate and low plasticity by measuring the areal surface roughness of notched specimens near the notch root at the initial stage of fatigue [9]. However, the surface roughness increases dramatically for majority of such materials at the intermediate and final stages of fatigue. Therefore, surface topology of notched specimens fabricated from these materials cannot be reconstructed near the notch root by single wavelength PSI due to the 2π ambiguity problem. To expand the range of the areal roughness measurements, we have developed the TS DWIM for retrieving surface relief up to $S_q \le \Lambda/10$. Theoretical description, computer simulation and experimental verification of the TS DWIM are represented in Sections 2, 3 and 4, respectively.

2. Two-step dual-wavelength interferometry method

The TS DWIM for a surface relief retrieving is based on a previously developed methods 1 and 2. These methods allow retrieving both a total relief of a smooth surface and its two components, namely a low-frequency surface relief and a high-frequency one. So, a PM $\varphi_R(i,j)$ of the total surface relief can be considered as the sum of a high-frequency PM $\varphi_H(i,j)$ and a low-frequency PM $\varphi_L(i,j)$, that is

$$\varphi_R(i,j) = \varphi_H(i,j) + \varphi_L(i,j) \tag{2}$$

where (i,j) are the image pixel coordinates ($0 \le i \le N-1$ and $0 \le j \le M-1$). In following symbols and equations the pixel coordinates (i,j) are omitted for brevity.

As in method 2, we propose to use two iterations of low-frequency and high-frequency PMs retrieval to decrease random and systematic errors and eliminate edge effects occurred at the fast Fourier transform (FFT) filtering.

In contrast to the single wavelength methods 1 and 2, the proposed TS DWIM uses not one but two interferogram pairs recorded for two different wavelengths λ_1 and λ_2, and each of them contains initial interferogram I_1 and interferogram I_2 with blind phase shift α of a reference wave ($0 < \alpha < \pi$), that is

$$I_1 = I_{obj} + I_{ref} + 2\sqrt{I_{obj} I_{ref}}\cos(\varphi_H + \varphi_L) = I_{obj} + I_{ref} + I_1' \tag{3}$$

$$I_2 = I_{obj} + I_{ref} + 2\sqrt{I_{obj} I_{ref}}\cos(\varphi_H + \varphi_L + \alpha) = I_{obj} + I_{ref} + I_2' \tag{4}$$

where I_{obj} and I_{ref} are the intensity distributions of the object and reference waves.

We should also register $I_{obj} = I_3$ and $I_{ref} = I_4$ for λ_1 and λ_2 to retrieve the PM φ_R.

To extract blind phase shift α, the correlation approach is applied [8, 10, 11]. According to it, a correlation coefficient ρ between two interferograms differed only by a blind phase shift α can be considered to be a cosine of this phase shift, that is

$$\alpha = \operatorname{acos}\left[\rho(I_1, I_2)\right] \tag{5}$$

So, if interferogram pairs (3) and (4) are recorded for wavelengths λ_1 and λ_2, blind phase shifts α_1 for λ_1 and α_2 for λ_2 can be found from Eq. (5).

If the phase shift α is known, a wrapped PM $[\varphi_R]_w$ of the total relief within the range $-\pi \le [\varphi_R]_w \le \pi$ that is extracted from (3) and (4) can be expressed as [10]

$$[\varphi_R]_w = [\varphi_H + \varphi_L]_w = \operatorname{atan}(I_1' \cos\alpha - I_2', I_1' \sin\alpha) \tag{6}$$

where $I_1' = I_1 - I_3 - I_4$ and $I_2' = I_2 - I_3 - I_4$. Equation (6) follows from the ratio [10]

$$\frac{I_2'}{I_1'} = \cos\alpha - \tan\varphi_R \sin\alpha \tag{7}$$

If wrapped PMs $[\varphi_R]_{w,\lambda_1}$ and $[\varphi_R]_{w,\lambda_2}$ for wavelengths λ_1 and λ_2 are calculated using Eq. (6), the difference wrapped PM for synthetic wavelength Λ is determined as

$$[\varphi_R]_{w,\Lambda} = [\varphi_R]_{w,\lambda_1} - [\varphi_R]_{w,\lambda_2} \tag{8}$$

where $\lambda_1 < \lambda_2$. This PM provides phase reconstruction in four quadrants within the range $-2\pi \le [\varphi_R]_{w,\Lambda} \le 2\pi$. In order to reduce this range twice to $-\pi \le [\varphi_R]'_{w,\Lambda} \le \pi$, the harmonic terms are used and a difference wrapped PM is expressed as

$$[\varphi_R]'_{w,\Lambda} = \operatorname{atan}\{\sin[\varphi_R]_{w,\Lambda}, \cos[\varphi_R]_{w,\Lambda}\} \tag{9}$$

First iteration of the PM $[\varphi_R]'_{w,\Lambda}$ processing, which is necessary to decrease random and systematic errors and remove influence of edge effects, includes the expansion of its dimensions in all four directions (vertical and horizontal). Computer simulation of a PM $[\varphi_{Ri}(k, l)]_{w,\Lambda}$ expansion has shown that it is enough to restrict the dimension by fifty rows from left and right sides ($0 \le k \le N + 99$) and fifty columns from bottom and top sides ($0 \le l \le M + 99$).

In order to produce an expanded wrapped low-frequency PM $[\varphi_L(k, l)]_w$, the expanded PM $[\varphi_{Ri}(k, l)]_{w,\Lambda}$ is processed by means of the well-known approach for reconstruction of harmonic components $I_s = \sin[\varphi_{Ri}(k, l)]_{w,\Lambda}$ and $I_c = \cos[\varphi_{Ri}(k, l)]_{w,\Lambda}$ [12]. Noniterative procedure for extraction $\sin[\varphi_L(k, l)]_{w,\Lambda}$ and $\cos[\varphi_L(k, l)]_{w,\Lambda}$ is realized by low-pass filtering in spatial frequency domain with application of FFT [9, 10], that is

$$\sin[\varphi_L(k, l)]_{w,\Lambda} \approx I_s[\varphi_L(k, l)]_{w,\Lambda} = \mathrm{FFT}^{-1}\left\{\mathrm{FFT}\left[\sin[\varphi_{Ri}(k, l)]_{w,\Lambda}\right] \times \mathrm{LPF1}\right\} \tag{10}$$

$$\cos[\varphi_L(k, l)]_{w,\Lambda} \approx I_c[\varphi_L(k, l)]_{w,\Lambda} = \mathrm{FFT}^{-1}\left\{\mathrm{FFT}\left[\cos[\varphi_{Ri}(k, l)]_{w,\Lambda}\right] \times \mathrm{LPF1}\right\} \tag{11}$$

where LPF1 is the low-pass filter. A cut-off frequency f_{c_0} of the LPF1 can be calculated as a maximum frequency of the wrapped PM $[\varphi_{Ri}(k, l)]_{w,\Lambda}$ saw tooth fringe structure. It can be found using the algorithm for estimation of a fringe orientation and fringe density proposed by YANG *et al*. [13]. Extracted harmonic components allow producing the expanded wrapped low-frequency PM, which can be written as

$$[\varphi_L(k, l)]_{w,\Lambda} = \operatorname{atan}\{I_s[\varphi_L(k, l)]_{w,\Lambda}, I_c[\varphi_L(k, l)]_{w,\Lambda}\} \tag{12}$$

After cutting the expanded map $[\varphi_L(k, l)]_{w,\Lambda}$, we obtain a PM $[\varphi_L(i, j)]_{w,\Lambda}$ with initial sizes. Unwrapping of this map allows producing the coarse low-frequency PM $[\varphi_L]_\Lambda$ at wavelength Λ as the first iteration result. Retrieving of a high-frequency coarse PM is performed by subtraction of the PM $[\varphi_L]_{w,\Lambda}$ from the difference wrapped map $[\varphi_R]_{w,\Lambda}$ expressed by Eq. (8), that is

$$[\varphi'_H]_\Lambda = [\varphi_R]_{w,\Lambda} - [\varphi_L]_{w,\Lambda} \tag{13}$$

This map contains singularity loci $[\varphi'_{\mathrm{H}}]_{\Lambda} = 2\pi$ and $[\varphi'_{\mathrm{H}}]_{\Lambda} = -2\pi$. The operations $I'_{\mathrm{s}} = \sin[\varphi'_{\mathrm{H}}]_{\Lambda}$ and $I'_{\mathrm{c}} = \cos[\varphi'_{\mathrm{H}}]_{\Lambda}$ [9, 10, 14] remove these singularities, and the improved coarse PM can be expressed as

$$[\varphi_{\mathrm{H}}]_{\Lambda} = \operatorname{atan}(I'_{\mathrm{s}}, I'_{\mathrm{c}}) \tag{14}$$

The improved coarse PM of the total relief is obtained after pixel-wise addition of the low-frequency and high-frequency PMs, that is

$$[\varphi_{\mathrm{R}\tilde{n}}]_{\Lambda} = [\varphi_{\mathrm{L}}]_{\Lambda} + [\varphi_{\mathrm{H}}]_{\Lambda} \tag{15}$$

This stage of the TS DWIM fulfillment completes its first iteration. The obtained improved coarse PM $[\varphi_{\mathrm{Rc}}]_{\Lambda}$ is used at the second iteration for extraction of an areal surface roughness fine PM φ_{A}. This procedure is dedicated for additional suppression of random and systematic errors presented in the PM $[\varphi_{\mathrm{R}c}]_{\Lambda}$ and separation of areal (3D) surface roughness and areal (3D) waviness from a total surface texture.

The second iteration is started from expansion of the PM $[\varphi_{\mathrm{R}c}(i, j)]_{\Lambda}$ dimensions to remove the influence of edge effects, which is similar to expansion of $[\varphi_{\mathrm{R}}(i, j)]_{\mathrm{w},\Lambda}$ at the first iteration. After expansion, the PM $[\varphi_{\mathrm{R}c}(k, l)]_{\Lambda}$ is subjected to spatial filtering by using the direct and inverse FFTs and low-frequency linear L-filter (see ISO 25178 -2012) LPF2, which is equivalent to cut-off filters used in 2D profilometry [15]. The nesting index frequency f_{c} that is equivalent to cut-off frequency for linear filters is significantly lower than the one for filter that is used at the first iteration. Choice of the frequency f_{c} depends on the test object surface texture. If we study an engineering surface by using linear filtering techniques, this frequency can be defined from cut-off wavelength $\lambda_{\mathrm{c}} = (f_{\mathrm{c}})^{-1}$. The wavelength λ_{c} is considered as the standardized parameter that qualifies a branch point between areal surface roughness and waviness components. An expanded filtered areal waviness PM $[\varphi_{\mathrm{W}}(k, l)]_{\Lambda}$ can be expressed as

$$[\varphi_{\mathrm{W}}(k, l)]_{\Lambda} = \mathrm{FFT}^{-1}\left\{\mathrm{FFT}\left[[\varphi_{\mathrm{R}\tilde{n}}(k, l)]_{\Lambda}\right] \times \mathrm{LPF2}\right\} \tag{16}$$

After cutting of the PM $[\varphi_{\mathrm{W}}(k, l)]_{\Lambda}$, we obtain a PM $[\varphi_{\mathrm{W}}(i, j)]_{\Lambda}$ with initial sizes.

Because the wrapped areal waviness PM is required for an areal roughness PM retrieval, the obtained PM $[\varphi_{\mathrm{W}}]_{\Lambda}$ is transformed into the wrapped one, that is

$$I''_{\mathrm{s}} = \sin[\varphi_{\mathrm{W}}]_{\Lambda} \tag{17a}$$

$$I''_{\mathrm{c}} = \cos[\varphi_{\mathrm{W}}]_{\Lambda} \tag{17b}$$

$$[\varphi_{\mathrm{W}}]_{\mathrm{w},\Lambda} = \operatorname{atan}(I''_{\mathrm{s}}, I''_{\mathrm{c}}) \tag{17c}$$

So, the areal roughness PM improved after second iteration is obtained as a difference between the wrapped PM $[\varphi_{\mathrm{R}}]'_{\mathrm{w},\Lambda}$ of a total surface relief expressed by Eq. (9), and the wrapped waviness PM $[\varphi_{\mathrm{W}}]_{\mathrm{w},\Lambda}$, *i.e.*,

$$[\varphi''_{\mathrm{A}}]_{\Lambda} = [\varphi_{\mathrm{R}}]'_{\mathrm{w},\Lambda} - [\varphi_{\mathrm{W}}]_{\mathrm{w},\Lambda} \tag{18}$$

At least, the areal surface roughness fine PM φ_A is extracted after realization of the similar procedure of singularity loci removal, that is

$$I_s''' = \sin[\varphi_A'']_{\Lambda} \tag{19a}$$

$$I_c''' = \cos[\varphi_A'']_{\Lambda} \tag{19b}$$

$$[\varphi_A]_{w,\Lambda} = \operatorname{atan}(I_s''', I_c''') \tag{19c}$$

Finally, a fine PM of the total relief is determined as

$$\varphi_R = [\varphi_W]_{\Lambda} + [\varphi_A]_{\Lambda} \tag{20}$$

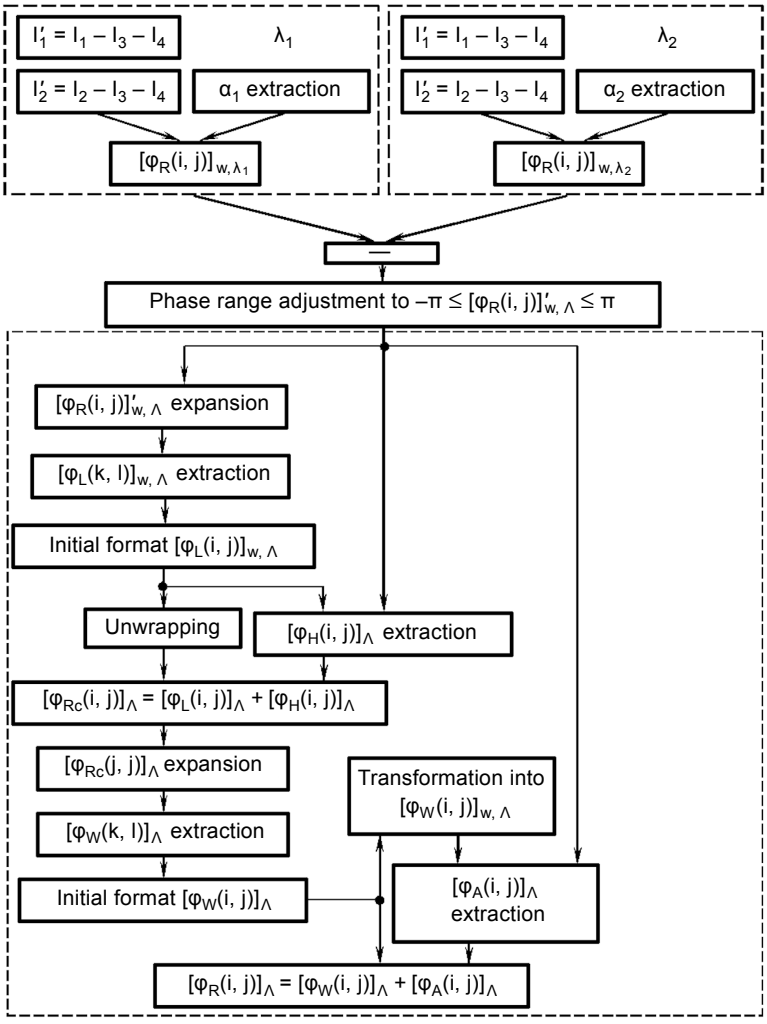

Fig. 1. Reduced flow graph of the interferogram processing.

Reduced flow graph of the proposed TS DWIM is shown in Fig. 1. Let us note that method 2 works in a similar way, in case of single wavelength.

Thus, due to implementation of low-frequency filtering and elimination of singularity loci in both iterations, the TS DWIM allows efficiently suppressing high-frequency and impulsive noises and obtaining fine PMs for wavelength Λ.

3. Computer simulation

Verification of the proposed method was fulfilled with three test phase images, namely a slope, a step, and a bipolar test object used to produce closed-fringe interferograms. These images are shown in Figs. 2**a**, 2**b** and 2**c**, respectively.

First test image is selected for demonstration of the proposed way of a wrapped PM range reduction by Eq. (9), which is simpler than the one shown in [4]. Second one (see Fig. 2**b**) is an unsolvable example of the surface relief retrieval for single-wavelength PSI. Third image represents a widely used test phase object that is described by computer function "3 peaks 500" (in GNU Octave) (see Fig. 2**c**). This object is convenient to estimate errors of a surface relief reconstruction. Phase changes $\Delta\varphi_p$ in these images are connected with their height changes Δh_p as $\Delta\varphi_p = 4\pi(\Delta h_p)/\lambda$ concerning to $\lambda_2 = 632.8$ nm. To evaluate the influence of areal surface roughness on a phase relief retrieval errors, the additive Gaussian phase noise with standard deviation (SD) σ_h was

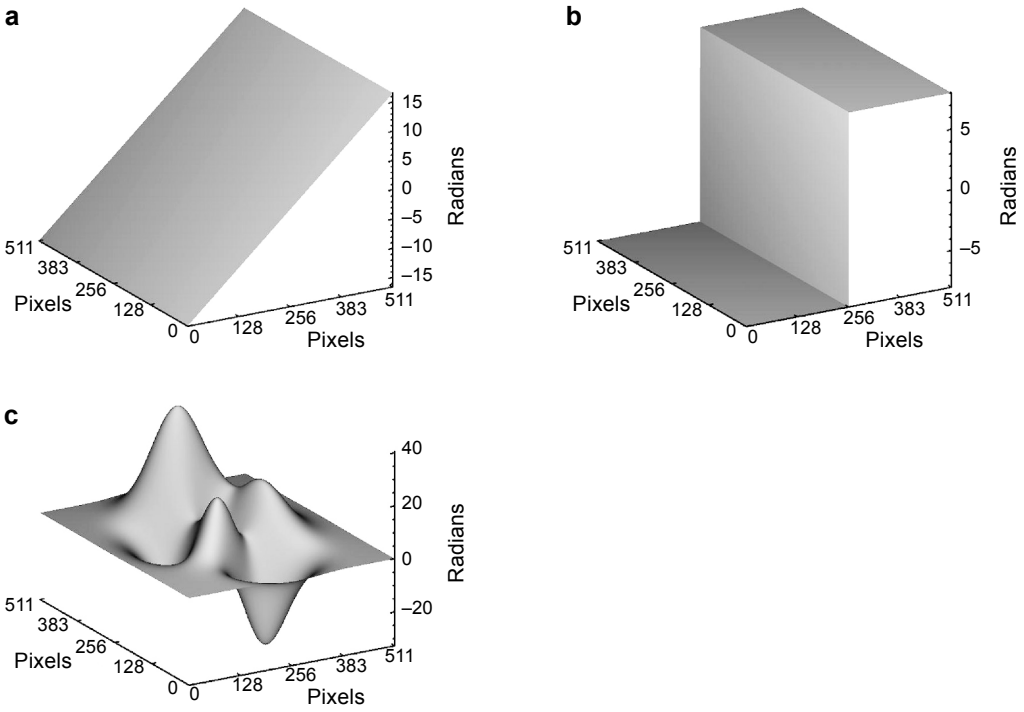

Fig. 2. Phase slope (**a**), phase step (**b**), and test phase object (**c**).

introduced to each test image. Wavelengths λ_1 = 532.0 nm and λ_2 = 632.8 nm were used for synthesis of two pairs of digital interferograms, respectively, that were produced according to Eqs. (3) and (4) with introducing of phase shifts α_1 for first pair and α_2 for second pair. For technical realization of the TS DWIM, it is the most convenient to have only one out-of-plane shift of a reference beam in order to record each second interferogram in two pairs. In this case, the ratio λ_2/λ_1 should be equal to ratio α_1/α_2. Because SD of the phase noise introduced into each test object is defined as $\sigma_{\varphi_1} = 4\pi(\sigma_h)/\lambda_1$ for wavelength λ_1 and $\sigma_{\varphi_2} = 4\pi(\sigma_h)/\lambda_2$ for wavelength λ_2, the ratio λ_2/λ_1 should be also equal to ratio $\sigma_{\varphi_2}/\sigma_{\varphi_1}$, that is

$$\lambda_2/\lambda_1 = \alpha_1/\alpha_2 \tag{21a}$$

$$\sigma_{\varphi_2}/\sigma_{\varphi_1} = \alpha_1/\alpha_2 \tag{21b}$$

Computer simulation results of several initial stages of the proposed TS DWIM fulfillment up to the stage inclusive evaluated by Eq. (8) during the phase slop (see Fig. 2**a**) retrieval are shown in Fig. 3. In this case, Gaussian phase noise's SDs equal to σ_{φ_1} = 0.373 rad and σ_{φ_2} = 0.314 rad and phase shifts α_1 = 35.68° and α_2 = 30.0° (λ_1 = 532.0 nm and λ_2 = 632.8 nm) were chosen in accordance with Eqs. (21). The smooth

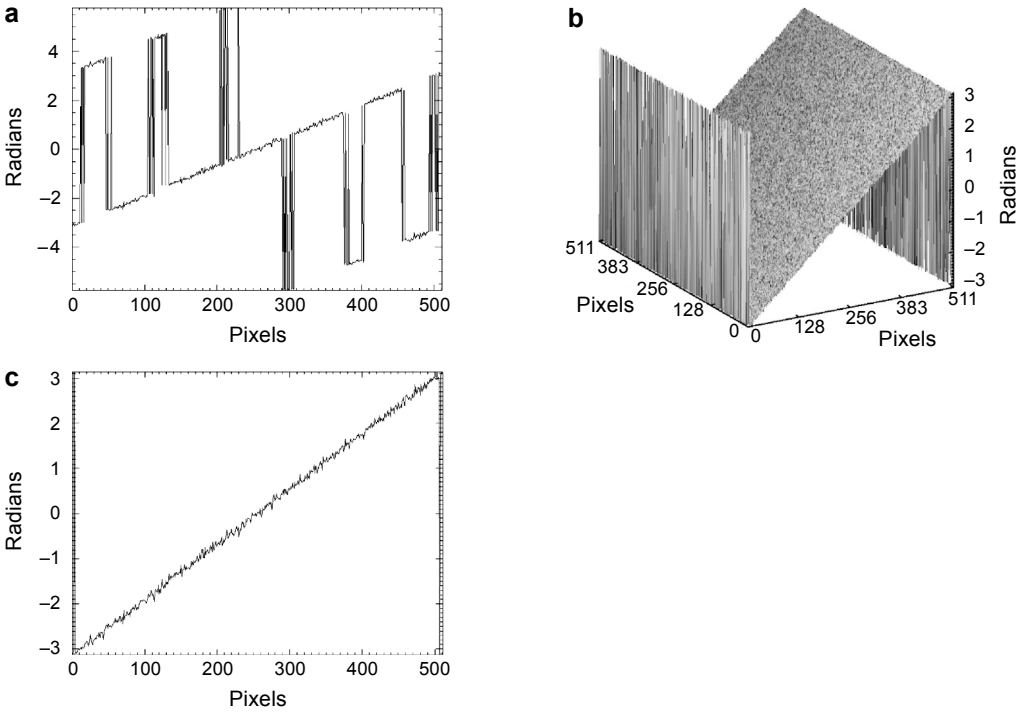

Fig. 3. Retrieval of the phase slope with Gaussian phase noise σ_{φ_2} = 0.314 rad: profile of PM $[\varphi_R(i,j)]_{w,\Lambda}$ for wavelength Λ = 3340 nm after fulfillment of the stage evaluated by Eq. (8) (**a**); isometric image of PM $[\varphi_R(i,j)]'_{w,\Lambda}$ after fulfillment of the stage evaluated by Eq. (9) (**b**) and its profile (**c**).

phase slope height has been chosen to provide one period of wavelength Λ for the retrieved PM. In this case, the second iteration and unwrapping are omitted. The phase noise σ_φ introduced into the smooth phase slope can be considered as a test RMS areal surface roughness $S_q = \lambda\sigma_\varphi/4\pi$ that corresponds to σ_{φ_2} as $S_{q_2} = \lambda_2/40 = 15.8$ nm. The histograms of error distributions of the surface relief retrieval for phase slopes with added Gaussian phase noises obtained at the range from $\sigma_{\varphi_2} = 0.314$ rad ($S_{q_2} = \lambda_2/40 = 15.8$ nm) to $\sigma_{\varphi_2^*} = 1.257$ rad ($S_{q_2^*} = \lambda_2/10 = 63.3$ nm) show that their half-widths decrease from 2.9×10^{-2} to 1.4×10^{-2} rad, if the surface roughness increases, which is agreed with results obtained and explained in [10, 11].

The developed method was also used for retrieval of a phase step exceeding 2π for both λ_1 and λ_2. Example of retrieval of the phase step equal to 805.7 nm or 19.03 rad for λ_1, 16.0 rad for λ_2 and 3.032 rad for Λ with added Gaussian phase noise emulating the surface roughness $S_{q_2^*} = \lambda_2/10 = 63.3$ nm is represented in Fig. 4. Obtained results show the effectiveness of the proposed TS DWIM to reconstruct phase slopes and phase steps of low-roughness surfaces.

The test phase object (see Fig. 2**c**) was used for more detailed estimation of surface roughness influence on errors of a surface relief retrieval by using the TS DWIM and methods 1 and 2. For this purpose, different RMS values S_q of Gaussian noise (from

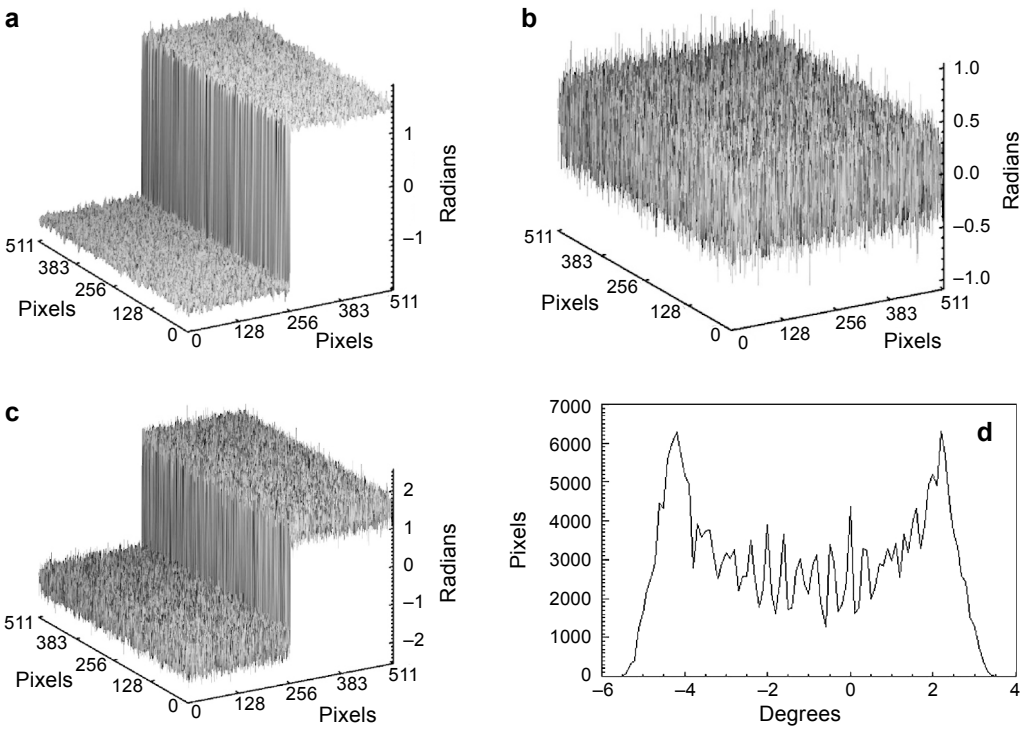

Fig. 4. Phase step retrieval with Gaussian phase noise $\sigma_{\varphi_2^*} = 1.257$ rad for $\Lambda = 3340$ nm: areal waviness PM $[\varphi_W(i,j)]_\Lambda$ (**a**), areal roughness PM $[\varphi_m(i,j)]_\Lambda$ (**b**), unwrapped total surface relief PM $[\varphi_R(i,j)]_\Lambda$ (**c**); histogram of error distribution of the phase step surface relief retrieval (**d**).

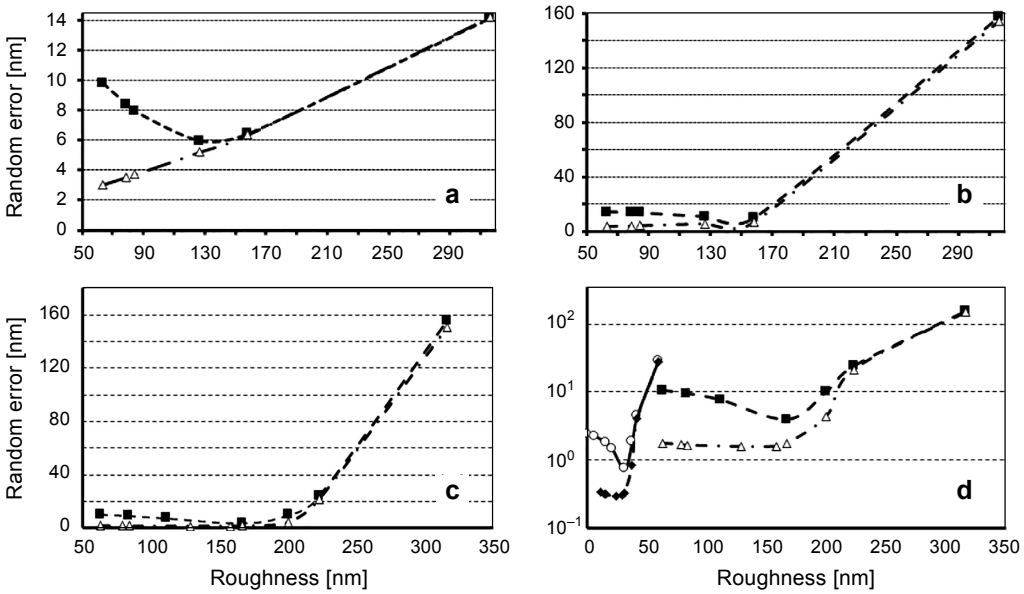

Fig. 5. Relationships between random errors and RMS areal waviness (**a**), RMS areal roughness (**b**), RMS total relief (**c**), and RMS roughness of a retrieved total relief (**d**). Dashed curve (samples are marked with squares) is obtained by method 1 for Λ = 3340 nm (**a**–**d**), dashed-dot one (samples are marked with triangle) is obtained by method 2 and TS DWIM for Λ = 3340 nm (**a**–**d**), solid one (samples are marked with circles) is obtained by method 1 for λ_2=632.8 nm (**d**), and dashed-dot one (samples are marked with diamonds) is obtained by method 2 for λ_2=632.8 nm (**d**).

$\lambda_2/10$ to $\lambda_2/2$ or from $1.895 \times 10^{-2}\Lambda$ to $9.474 \times 10^{-2}\Lambda$) emulating surface roughness were added to this test object. Results of retrieval of phase relief with different roughness values have allowed determining the dependences "random error *vs.* roughness" for wavelength Λ = 3340 nm, which are represented in Figs. 5**a**–5**c**. Because the procedures of the TS DWIM and single wavelength method 2 fulfillment are similar, the indicated dependences obtained by these methods are the same. These figures also show that the total surface relief random errors covering the range from S_q = 60 nm to S_q = 316 nm are lesser than the similar random errors of the areal roughness, because there is the strict negative interrelationship between random errors of retrieved areal roughness and waviness PMs, as it is shown in [10]. Retrieval of the test object reliefs with RMS areal roughness values up to $S_q \le 79.1$ nm was fulfilled also by methods 1 and 2 for wavelength λ_2 = 632.8 nm. The dependences "random error *vs.* RMS roughness of a retrieved total relief" obtained by using methods 1 and 2 are shown in Fig. 5**d** as solid and dashed-dot curves (samples are marked with circles and diamonds), respectively. Let us note that random errors of the total surface relief retrieved by method 2 are lesser than ones of the same relief retrieved by method 1. A comparison of these dependences with the ones obtained by the TS DWIM for Λ = 3340 μm (see Fig. 5**c**) shows that methods 1 and 2 can retrieve surface reliefs with RMS areal roughness up to $S_q \approx \lambda_2/8$ (or $S_q \approx \lambda_1/8$), and the proposed TS DWIM – up to $S_q \approx \Lambda/8$. So, the allowable

random errors of these reliefs retrieval can be provided by methods 1 and 2 for λ_1 = 532.0 nm and λ_2 = 632.8 nm, if $S_q \le 70$ nm, and by the TS DWIM, if 60 nm $\le S_q \le$ 300 nm.

Analysis of obtained dependences "systematic error *vs.* surface roughness" has shown that the influence of these errors on the total errors is very small.

The processing time to retrieve final fine PMs of test objects with a display of ten intermediate images is equal to 4.8 s, if the 200 MHz computer and the Visual IDL Programming is used. This time is equivalent to a time of about 0.15 s, if a 2.8 GHz computer is used for processing of a test object with a size of 256 × 256 pixels. A comparison with such well-known 5-step DW interferometry approaches as simultaneous phase-shifting dual-wavelength interferograms, single-wavelength phase-shifting, and temporal Fourier transform shows that their processing times are larger (0.187, 0.485, and 11.83 s, respectively) for a 2.8 GHz laptop and the test object with the same size of 256 × 256 pixels [16].

4. Experimental verification

To verify the TS DWIM, the experimental setup based on a two-wavelength Twyman –Green phase-shifting interferometer optical scheme was developed (see Fig. 6). In this scheme, the synthetic wavelength Λ = 24.2 μm was generated with He-Ne laser (λ_1 = 633 nm) and a laser diode (λ_2 = 650 nm). Because the laser diode coherence length is equal about 4 mm, the scheme was carefully adjusted to align optical paths from laser sources to a CCD-camera with pixel pitch equal to 4.65 μm. The lateral magnification M = 1.5 for recording of interferograms was chosen according to approach proposed in [9, 14]. The rough surface of a cast iron specimen corresponding to the 6th grade of roughness (purity) according to GOST was chosen as a test object. During the experiment, two pairs of interferograms and object and reference wavefronts for two wavelengths were recorded. The second pair of interferograms was recorded at the same longitudinal shift of the reference wave, which corresponds to phase shifts equal to 61.2° for λ_1 and 59.6° for λ_2 concerning the first pair (see Eqs. (21)). Retrieved

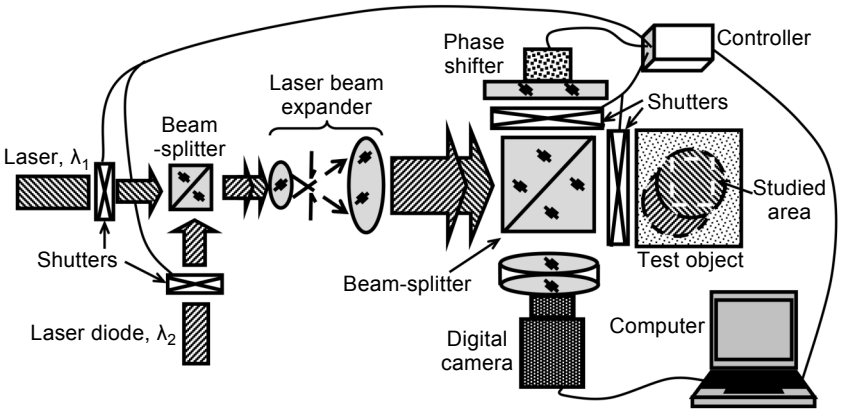

Fig. 6. Schematic diagram of an experimental setup.

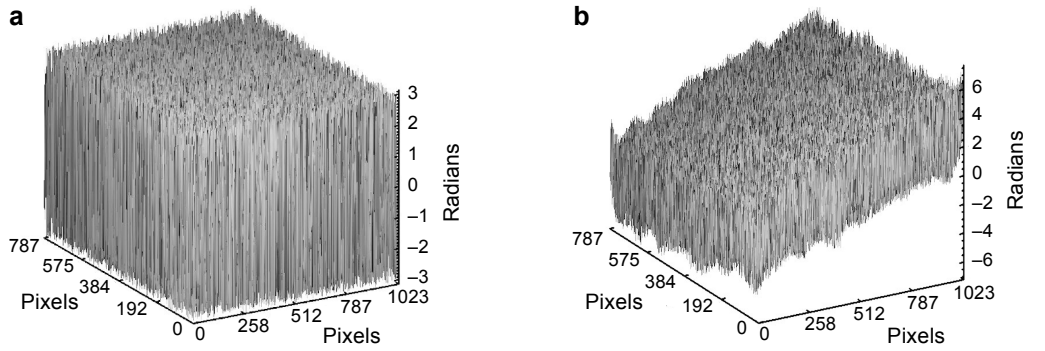

Fig. 7. Reconstruction of the chosen area (3.17 × 2.38 mm^2) of the cast iron specimen rough surface possessing 6th grade of roughness: PM of 3D surface roughness (**a**), and PM of total surface relief (**b**).

fine PMs of 3D surface roughness and total relief of the chosen area of dimensions equal to 1024 × 768 pixels are shown in Fig. 7. We have calculated the roughness average R_a along several profiles of both the retrieved 3D roughness and total surface relief, which PMs are represented in Fig. 7. As a result, $R_{a_1} = 2.51$ μm in metric units for the 3D roughness PM represented in Fig. 7**a**; and $R_{a_2} = 2.74$ μm and roughness ten point height $R_{z_2} = 10.72$ μm for the total surface relief PM represented in Fig. 7**b**. These results correspond to actual roughness values of the studied test object.

5. Conclusion

The proposed TS DWIM allows widening the measurement range of rough surfaces by using only four interferograms and realizing only one out-of-plane blind phase shift of a reference wave. In comparison with method 1 allowing retrieval of areal surface textures, which RMS areal roughness $S_q \le \lambda_1/8$ or $S_q \le \lambda_2/8$, the TS DWIM can retrieve surfaces, which RMS areal roughness reaches $S_q \approx \Lambda/8$. Method 2 provides lesser random errors of surface relief retrieval in comparison with method 1 and possesses the same random errors as the TS DWIM. However, it retrieves such areal surface textures, which RMS areal roughness is not exceeding $\lambda_1/8$ or $\lambda_2/8$. Computer simulation has shown the possibility of the proposed TS DWIM to retrieve standard test objects with introduced Gaussian noise emulating the surface relief. The TS DWIM performance is estimated by error analysis for wide range of areal surface roughness changes. The experiments proved the validity of the TS DWIM.

References

[1] CHENG Y.-Y., WYANT J.C., *Two-wavelength phase shifting interferometry*, Applied Optics **23**(24), 1984, pp. 4539–4543, DOI: 10.1364/AO.23.004539.

[2] COCHRAN E.R., CREATH K., *Combining multiple-subaperture and two-wavelength techniques to extend the measurement limits of an optical surface profiler*, Applied Optics **27**(10), 1988, pp. 1960–1966, DOI: 10.1364/AO.27.001960.

[3] PARSHALL D., KIM M.K., *Digital holographic microscopy with dual-wavelength phase unwrapping*, Applied Optics **45**(3), 2006, pp. 451–459, DOI: 10.1364/AO.45.000451.

[4] TAY C.J., QUAN C., NIU H., BHADURI B., *Phase retrieval in two-wavelength DSSI using a combined filtering method*, Optik **122**(23), 2011, pp. 2114–2118, DOI: 10.1016/j.ijleo.2011.01.007.

[5] XIAOQING XU, YAWEI WANG, YUANYUAN XU, WEIFENG JIN, *Dual-wavelength in-line phase-shifting interferometry based on two dc-term-suppressed intensities with a special phase shift for quantitative phase extraction*, Optics Letters **41**(11), 2016, pp. 2430–2433, DOI: 10.1364/OL.41.002430.

[6] XIAOQING XU, YAWEI WANG, YING JI, YUANYUAN XU, MING XIE, HAO HAN, *A novel dual-wavelength iterative method for generalized dual-wavelength phase-shifting interferometry with second-order harmonics*, Optics and Lasers in Engineering **106**, 2018, pp. 39–46, DOI: 10.1016/j.optlaseng.2018.02.007.

[7] KUMAR U.P., BHADURI B., KOTHIYAL M.P., MOHAN N.K., *Two-wavelength micro-interferometry for 3-D surface profiling*, Optics and Lasers in Engineering **47**(2), 2009, pp. 223–229, DOI: 10.1016/j.optlaseng.2008.04.005.

[8] MURAVSKY L.I., OSTASH O.P., KMET' A.B., VORONYAK T.I., ANDREIKO I.M., *Two-frame phase-shifting interferometry for retrieval of smooth surface and its displacements*, Optics and Lasers in Engineering **49**(3), 2011, pp. 305–312, DOI: 10.1016/j.optlaseng.2010.11.021.

[9] MURAVSKY L., PICART P., KMET' A., VORONYAK T., OSTASH O., STASYSHYN I., *Evaluation of fatigue process zone dimensions in notched specimens by two-step phase shifting interferometry technique*, Optical Engineering **55**(10), 2016, article ID 104108, DOI: 10.1117/1.OE.55.10.104108.

[10] MURAVSKY L.I., KMET' A.B., VORONYAK T.I., *Retrieving the relief of a low-roughness surface using a two-step interferometric method with blind phase shift of a reference wave*, Optics and Lasers in Engineering **50**(11), 2012, pp. 1508–1516, DOI: 10.1016/j.optlaseng.2012.06.011.

[11] MURAVSKY L., KMET' A., VORONYAK T., *Two approaches to the blind phase shift extraction for two-step electronic speckle pattern interferometry*, Optical Engineering **52**(10), 2013, article ID 101909, DOI: 10.1117/1.OE.52.10.101909.

[12] AEBISCHER H.A., WALDNER S., *A simple and effective method for filtering speckle-interferometric phase fringe patterns*, Optics Communications **162**(4–6), 1999, pp. 205–210, DOI: 10.1016/S0030-4018(99)00116-9.

[13] XIA YANG, QIFENG YU, SIHUA FU, *An algorithm for estimating both fringe orientation and fringe density*, Optics Communications **274**(2), 2007, pp. 286–292, DOI: 10.1016/j.optcom.2007.02.020.

[14] MURAVSKY L.I., KMET' A.B., STASYSHYN I.V., VORONYAK T.I., BOBITSKI Y.V., *Three-step interferometric method with blind phase shifts by use of interframe correlation between interferograms*, Optics and Lasers in Engineering **105**, 2018, pp. 27–34, DOI: 10.1016/j.optlaseng.2017.12.011.

[15] RAJA J., MURALIKRISHNAN B., SHENGYU FU, *Recent advances in separation of roughness, waviness and form*, Precision Engineering **26**(2), 2002, pp. 222–235, DOI: 10.1016/S0141-6359(02)00103-4.

[16] WANGPING ZHANG, XIAOXU LU, LEIHUAN FEI, HUI ZHAO, HANLING WANG, LIYUN ZHONG, *Simultaneous phase-shifting dual-wavelength interferometry based on two-step demodulation algorithm*, Optics Letters **39**(18), 2014, pp. 5375–5378, DOI: 10.1364/OL.39.005375.

Received October 25, 2017
in revised form May 27, 2018